Coastal Dynamics 2017
Paper No. 141

AN INTEGRATED MATHEMATICAL MODEL FOR THE DESIGN OF COASTAL PROTECTION STRUCTURES

Theofanis V. Karambas[1] and Achilleas G. Samaras[1,2]

Abstract

In the present work an integrated coastal engineering numerical model is presented. The model simulates the linear wave propagation, wave induced circulation, sediment transport and bed morphology evolution. It consists of three main modules: WAVE_L, WICIR and SEDTR. The nearshore wave transformation module WAVE_L (WAVE_Linear) is based on the hyperbolic-type mild slope equation and is valid for a compound linear wave field near coastal structures where the waves are subjected to the combined effects of shoaling, refraction, diffraction, reflection (total and partial) and breaking. Radiation stress components (calculated from WAVE_L) drive the depth averaged circulation module WICIR (Wave Induced CIRculation) for the description of the nearshore wave-induced currents. Sediment transport and bed morphology evolution in the nearshore, surf and swash zone are simulated by the SEDTR (SEDiment TRansport) module.

Key words: waves, coastal protection structures, sediment transport, morphology evolution, numerical model.

1. Introduction

Numerical models are nowadays the main tool for coastal engineers involved in the design of coastal/marine structures, with their advanced capabilities covering all aspects of wave-, hydro- and morpho-dynamics from deep water to the nearshore. Accurate numerical modelling of water wave propagation from offshore to coastal regions is of paramount importance to coastal, port and environmental engineers. Such models can greatly simplify and expedite the design of coastal structures and the evaluation of their influence on the surrounding environment. An integrated approach includes also the estimation of the wave induced current field, the sediment transport and the bottom topography changes in the coastal areas due to the action of the waves.

This work presents an integrated coastal engineering numerical model that simulates linear wave propagation, wave-induced circulation, sediment transport and bed morphology evolution. The model is tested against bed morphology evolution data (both laboratory and field measurements) in the presence of coastal protection structures. Its performance is considered to be overall quite satisfactory, supporting the rationale behind its use in relevant coastal engineering applications.

2. Model description

The proposed model consists of three main modules: (a) the linear wave propagation module WAVE_L; (b) the wave-induced circulation module WICIR; and (c) the sediment transport and bed morphology evolution module SEDTR.

2.1. *Nearshore wave transformation module – WAVE_L*

Linear wave propagation is simulated by applying a mild-slope model (Copeland, 1985a, Watanabe and Maruyama, 1986), derived without the assumption of progressive waves. The module WAVE_L is based on the hyperbolic-type mild slope equation and is valid for a compound wave field near coastal structures

[1]Department of Civil Engineering, Aristotle University of Thessaloniki, University Campus, 56 424, Thessaloniki, Greece. karambas@civil.auth.gr / asamaras@civil.auth.gr

where the waves are subjected to the combined effects of shoaling, refraction, diffraction, reflection (total and partial) and breaking. The module consists of the following pair of equations (Copeland, 1985a, Watanabe and Maruyama, 1986):

$$\frac{\partial \eta}{\partial t} + \frac{c}{c_g} \nabla \frac{c_g}{c} \mathbf{Q}_w = 0 \qquad \frac{\partial \mathbf{U}_w}{\partial t} + \frac{c^2}{d} \nabla \eta = \nu_h \nabla^2 \mathbf{U}_w \tag{1}$$

where η is the surface elevation, $\mathbf{U_w}$ the mean velocity vector $\mathbf{U_w}=(U_w, V_w)$, d the depth, $\mathbf{Q_w}=\mathbf{U_w}\ h_w=(Q_w, P_w)$, h_w the total depth ($h_w=d+\eta$), c the celerity and c_g the group velocity. The term ν_h is an horizontal eddy viscosity coefficient introduced in order to include breaking effects based on the formulation of Battjes (1975):

$$\nu_h = 2d\left(\frac{D}{\rho}\right)^{1/3} \tag{2}$$

where D is the dissipation of wave energy expressed as:

$$D = \frac{1}{4} Q_b f \rho g H_m^2 \tag{3}$$

where H_m is the maximum wave height, ρ the water density, f the wave frequency, and Q_b the probability for a wave to break at a depth, expressed as $(1-Q_b)/(\ln Q_b)=(H_{rms}/H_m)^2$ according to Battjes and Janssen (1978). The mean square wave height H_{rms} is calculated from $H_{rms}=2\ (<2\eta^2>)^{1/2}$, with the brackets denoting a time-mean quantity. It should be noted that – since linear wave models are not capable of describing waves in the swash zone – in WAVE_L the water depth from the rundown point (i.e. depth equal to $R/4$; R is the runup height) and up to the runup point (i.e. depth equal to $-R$) is considered to be constant and equal to $R/4$.

WAVE_L is adapted for engineering applications based on the following:

1. The input wave is introduced at a line inside the computational domain according to Larsen and Dancy (1983) and Lee and Suh (1998).
2. A sponge layer boundary condition is used to absorb the outgoing waves at the four sides of the domain (Larsen and Dancy, 1983).
3. The presence of vertical structures is incorporated by introducing a total reflection boundary condition ($U_w=0$ or $V_w=0$).
4. Partial reflection is also simulated, by introducing an artificial eddy viscosity coefficient ν_h. The values of ν_h are estimated from the method developed by Karambas and Bowers (1996), using the reflection coefficient values proposed by Bruun (1985).
5. The presence of submerged structures is incorporated as in Kriezi and Karambas (2004).
6. The presence of floating structures is incorporated as in Koutandos et al. (2004).

The numerical solution is based on the well-documented explicit second order finite difference staggered scheme using a mid-time method (Watanabe and Maruyama, 1986).

2.2. *Wave-induced circulation module – WICIR*

The depth and shortwave-averaged 2D continuity and momentum equations are used for simulating nearshore currents in the coastal zone. Based on linear wave theory, Copeland, (1985b) derived the equations for radiation stresses (S_{ij}) without the typical assumption of progressive waves, expressed as:

$$\frac{S_{xx}}{\rho} = d^2 < U_w^2 > A_r - d^2 < \left(\frac{\partial U_w}{\partial x} + \frac{\partial V_w}{\partial y} \right)^2 > B_r + \frac{\partial}{\partial x} < \left[U_w \left(\frac{\partial U_w}{\partial x} + \frac{\partial V_w}{\partial y} \right) \right] > D_r + \frac{\partial}{\partial y} < \left[V_w \left(\frac{\partial U_w}{\partial x} + \frac{\partial V_w}{\partial y} \right) \right] > D_r + \frac{1}{2} g < \eta^2 > \tag{4}$$

$$\frac{S_{yy}}{\rho} = d^2 < V_w^2 > A_r - d^2 < \left(\frac{\partial U_w}{\partial x} + \frac{\partial V_w}{\partial y} \right)^2 > B_r + d^2 \frac{\partial}{\partial y} < \left[V_w \left(\frac{\partial U_w}{\partial x} + \frac{\partial V_w}{\partial y} \right) \right] > D_r + d^2 \frac{\partial}{\partial x} < \left[U_w \left(\frac{\partial U_w}{\partial x} + \frac{\partial V_w}{\partial y} \right) \right] > D_r + \frac{1}{2} g < \eta^2 > \tag{5}$$

$$\frac{S_{xy}}{\rho} = d^2 < U_w V_w > A_r \tag{6}$$

$$A_r = \frac{k}{4 \sinh^2 kd} \left(\sinh 2kd + 2kd \right) \qquad B_r = \frac{1}{4k \sinh^2 kd} \left(\sinh 2kd - 2kd \right) \tag{7}$$

$$D_r = \frac{d}{4 \sinh^2 kd} \left(\frac{1}{2kd} \sinh 2kd - \cosh 2kd \right) \tag{8}$$

where k is the wave number and the brackets denote a time-mean quantity.

In nearshore circulation models the treatment of the bottom stress is critical. The bottom shear stresses $\boldsymbol{\tau_b}=(\tau_{bx}, \tau_{by})$ in WICIR are calculated based on the formulae proposed by Kobayashi et al. (2007):

$$\tau_{bx} = \frac{1}{2} \rho f_b \sigma_T^2 G_{bx} \qquad \tau_{by} = \frac{1}{2} \rho f_b \sigma_T^2 G_{by} \tag{9}$$

$$G_{bx} = \frac{U}{\sigma_T} \left[1.16^2 + \left(\frac{U}{\sigma_T} \right)^2 \right]^{0.5} \qquad G_{by} = \frac{V}{\sigma_T} \left[1.16^2 + \left(\frac{V}{\sigma_T} \right)^2 \right]^{0.5} \tag{10}$$

where f_b is the bottom friction factor, σ_T is the standard deviation of the oscillatory horizontal velocity, and U,V are the depth-averaged current velocities.

Since acting as the "link" between WAVE_L and SEDTR in the framework of the proposed integrated model, it is important for WICIR to be able to reproduce a number of processes that are essential for the realistic description of sediment transport.

Regarding the surf zone, it should be noted that the existence of the undertow (i.e. the current directed offshore) cannot be directly predicted by depth-averaged models; nonetheless, its representation is essential in the aforementioned context. In WICIR, quasi-3D effects are introduced by adopting the analytical expression for the vertical distribution of the cross-shore flow below wave trough level proposed by Stive and Wind (1986), expressed as:

$$v_u = \frac{1}{2} \left[\left(\xi - 1 \right)^2 - \frac{1}{3} \right] \frac{h - \zeta_t}{\rho \, \nu_\tau} \frac{dR}{dy} + \left(\xi - \frac{1}{2} \right) \frac{\left(h - \zeta_t \right) \tau_s}{\rho \nu_\tau} - \frac{M \cos \Theta}{h - \zeta_t} \tag{11}$$

where v_u is the undertow velocity in the direction normal to the shore, $h=d+\zeta$ (ζ being the mean water elevation), $dR/dy=0.14\rho g d h/dy$, τ_s is the shear stress at the wave trough level, M the wave mass flux above trough level (including surface roller effects), Θ the direction of wave propagation ($\Theta=\arctan[(<Q_w^2>/<P_w^2>)^{1/2}]$), and ν_τ the eddy viscosity coefficient according to De Vriend and Stive (1987):

$$\nu_\tau = 0.025 \, h \left(\frac{D}{\rho} \right)^{1/3} \tag{12}$$

Regarding the swash zone, an essential process for shoreline evolution is longshore sediment transport. For obliquely incident waves the trajectory of the bore-front follows a parabolic movement in the swash, following the direction of the net longshore flow per wave period. The mean longshore transport velocity V_R at the shoreline is determined according to Baba and Camenen (2007) as:

$$V_R = \sqrt{2\,g\,R}\,\sin\Theta \tag{13}$$

where R is the runup height and Θ is the wave direction near the rundown point at depth d=R/4. The longshore velocity V_R is presumed constant within the swash zone, the width of which is considered as extending from d=R/4 (i.e. the rundown point) to d=-R. The above velocity is indirectly introduced in the model by increasing the radiation stresses in the swash zone. Comparison of (13) to analytical expressions of longshore velocity, identified that – in the above context – radiation stresses have to be multiplied by a factor, a_s, given by:

$$a_s = 16\sqrt{\gamma\,\xi^{1.8}\left(H_o / L_o\right)^{0.2}} \tag{12}$$

where γ is the breaking index, ξ is the Irribaren number, and H_0, L_0 are the wave height and wavelength, respectively, for deep water conditions.

Finally, regarding flooding due to wave setup, in WICIR this process is simulated using the "dry bed" boundary condition which, according to Militello et al. (2004), at a given grin point (i,j) can be written as the following set of pairs of conditions:

if $(d+\zeta)_{i,j} > h_{cr}$ and $(d+\zeta)_{i-1,j} \le h_{cr}$ and $U_{i,j}>0 \rightarrow U_{i,j}=0$
if $(d+\zeta)_{i,j} > h_{cr}$ and $(d+\zeta)_{i,j-1} \le h_{cr}$ and $V_{i,j}>0 \rightarrow V_{i,j}=0$

if $(d+\zeta)_{i,j} \le h_{cr}$ and $(d+\zeta)_{i-1,j} \le h_{cr} \rightarrow U_{i,j}=0$
if $(d+\zeta)_{i,j} \le h_{cr}$ and $(d+\zeta)_{i,j-1} \le h_{cr} \rightarrow V_{i,j}=0$

if $(d+\zeta)_{i,j} \le h_{cr}$ and $(d+\zeta)_{i-1,j} > h_{cr}$ and $U_{i,j}<0 \rightarrow U_{i,j}=0$
if $(d+\zeta)_{i,j} \le h_{cr}$ and $(d+\zeta)_{i,j-1} > h_{cr}$ and $V_{i,j}<0 \rightarrow V_{i,j}=0$

where ζ is the mean water surface elevation and h_{cr} is a terminal depth below which drying is assumed to occur (e.g. in WICIR this depth is set to h_{cr}=0.001 m).

The numerical solution in WICIR is – as also in WAVE_L – based on the explicit second order finite difference staggered scheme using a mid-time method (Watanabe and Maruyama, 1986).

2.3. *Sediment transport module – SEDTR*

The mode of sediment movement on the coast is usually divided into bed load, suspended load and sheet flow transport. Different model concepts are being presently used for the prediction of each one, which range from empirical transport formulae to more sophisticated bottom boundary layer models. In the present work, the bed load transport (q_b) is estimated with a quasi-steady, semi-empirical formulation, developed by Camenen, and Larson, (2007, 2008) for an oscillatory flow combined with a superimposed current under an arbitrary angle:

$$\Phi_b = \begin{cases} \dfrac{q_{b,w}}{\sqrt{(s-1)\,g\,d_{50}^{\,3}}} = a_n\sqrt{\theta_{cw,net}}\,\theta_{cw,m}\exp\left(-b\,\dfrac{\theta_{cr}}{\theta_{cw}}\right) \\ \dfrac{q_{b,n}}{\sqrt{(s-1)\,g\,d_{50}^{\,3}}} = a_n\sqrt{\theta_{cn}}\,\theta_{cw,m}\exp\left(-b\,\dfrac{\theta_{cr}}{\theta_{cw}}\right) \end{cases} \tag{13}$$

where the subscripts *w* and *n* correspond, respectively, to the wave direction and the direction normal to the wave direction, *s* (= ρ_s/ρ) is the relative density between sediment (ρ_s) and water (ρ), *g* the acceleration due to gravity, d_{50} the median grain size, a_w, a_n and *b* are empirical coefficients, $\theta_{cw,m}$ and θ_{cw} the mean and maximum Shields parameters due to wave-current interaction, θ_{cn} the current-related Shields parameter in the direction normal to the wave direction, and θ_{cr} the critical Shields parameter for the inception of transport. The net Shields parameter $\theta_{cw,net}$ in Eq.(13) is given by:

$$\theta_{cw,net} = \left(1-a_{pl,b}\right)\left(1+a_{\alpha}\right)\theta_{cw,on} - \left(1+a_{pl,b}\right)\left(1-a_{\alpha}\right)\theta_{cw,off} \tag{14}$$

where $\theta_{cw,on}$ and $\theta_{cw,off}$ are the mean values of the instantaneous Shields parameter over the two half "periods" T_{wc} (crest-onshore) and T_{wt} (trough-offshore), $\alpha_{pl,b}$ a coefficient for the phase-lag effects (Camenen and Larson, 2007) and α_{α} a coefficient for the acceleration effects (Camenen and Larson 2006). The Shields parameter θ_{cw} is defined by:

$$\theta_{cw,j} = \tfrac{1}{2} f_{cw} U_{cw,j}^2 / \left[(s-1) g d_{50}\right] \tag{15}$$

with U_{cw} being the wave and current velocity, f_{cw} the friction coefficient taking into account wave and current interaction, while the subscript *j* should be replaced either by *onshore* or *offshore*. In the above formulation (since linear wave theory cannot be used) the estimation of nonlinear time-varying near-bottom wave velocities is needed as well. For the incorporation of nonlinear velocity characteristics (i.e. skewness and asymmetry) in SEDTR, the parameterisation proposed by Isobe and Horikawa (1982) is adopted.

The incorporation of the suspended sediment transport rate in SEDTR is done by solving the depth-integrated transport equation for suspended sediment (Kobayashi and Tega, 2002, Nam et al., 2009):

$$\frac{\partial(hC)}{\partial t} + \frac{\partial(hCU)}{\partial x} + \frac{\partial(hCV)}{\partial x} = c_R w_s - w_s \frac{C}{\beta_d} \tag{16}$$

where *h* is the total mean depth, *C* the depth-averaged volumetric sediment concentration, c_R the reference concentration at the bottom (Camenen and Larson, 2007), w_s the sediment fall velocity, and β_d is a coefficient calculated based on Camenen and Larson (2008) by:

$$\beta_d = \frac{\varepsilon}{w_s}\left[1 - \exp\left(-\frac{w_s h}{\varepsilon}\right)\right] \tag{17}$$

with ε being the sediment diffusivity (related to the eddy viscosity coefficient), estimated by (De Vriend and Stive, 1987):

$$\varepsilon = 0.025\, h\, \left(D/\rho\right)^{1/3} \tag{18}$$

Cross-shore sediment transport in the swash zone in SEDTR is calculated according to Larson and Wamsley (2007), while for the longshore sediment transport only the increased mean velocity is taken into account, as described in Section 2.2.

These sediment transport rates are then used for the simulation of the coastal bathymetry changes by the module SEDTR. The methodology adopted for the series of model applications, can be encoded into the steps described in the following. First, the initial bathymetry is inserted into the wave and wave-induced circulation modules (WAVE_L and WICIR, respectively) in order to estimate the wave and current fields. These fields are afterwards used by the sediment transport module SEDTR to calculate the sediment transport rates. Finally, bathymetry is updated by SEDTR solving the equation of the conservation of sediment transport (for the previously calculated transport rates). The procedure is repeated for a user-specified time period or until a state of morphologic equilibrium is reached.

3. Model applications

3.1. *Comparison with experimental data*

The integrated numerical model was set-up and applied in order to reproduce the small scale experiments of: (a) Ming and Chiew (2000), who studied the shoreline changes caused by the presence of a detached breakwater under the influence of pure wave action (laboratory measurements); and (b) Badiei et al. (1995), who studied the morphological effects of groins on an initially straight beach exposed to oblique irregular waves (laboratory measurements).

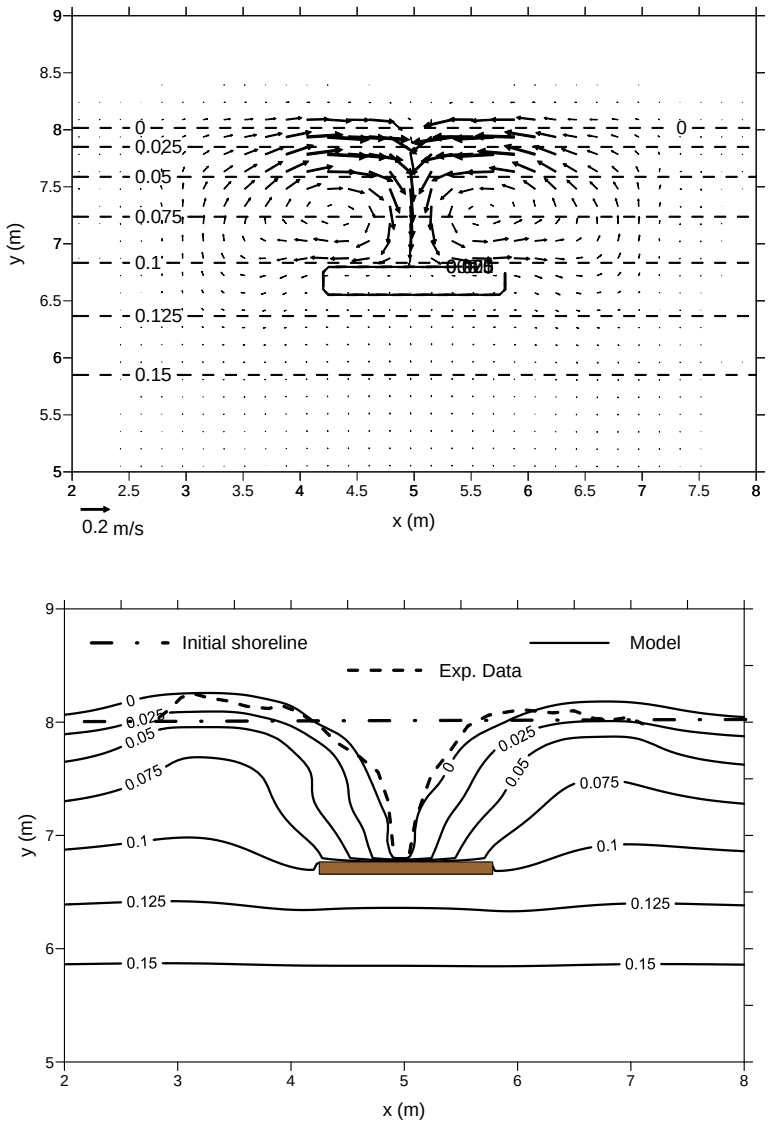

Figure 1: Wave-induced current velocity field (top) and comparison between the computed and measured shoreline and bathymetry evolution (bottom) for Test 11 of Ming and Chiew (2000).

The experiments of Ming and Chiew (2000) were conducted in a 10 m long, 5 m wide and 0.7 m high wave basin. A plunger-type wavemaker was used to generate monochromatic waves. Sponge was placed behind the wavemaker to minimize wave reflection. The 6 m long beach consisted of uniformly distributed sand with a median grain size of d_{50} = 0.25 mm. The tests duration was approximately 15 h (which was the duration needed for the beach to reach an equilibrium state as well). Three different cases were reproduced

numerically and are presented in the following, for normally incident waves of H_0=0.05 m deep water wave height and T=0.85 s wave period. The test cases, presented in Table 1, differed in breakwater length (B) and breakwater distance from the initial shoreline (X), in order to cover a wide range of B/X ratios resulting in both tombolo and salient formation behind the breakwaters.

Table 1. Experimental test conditions

Test	B=Breakwater length (m)	X=Distance from the initial shoreline (m)	B/X	Formation of salient/tombolo
3	1.5	0.6	2.50	tombolo
10	0.9	0.9	1.00	salient
11	1.5	1.2	1.25	tombolo

Figure 1 shows the wave-induced current velocity field and the comparison between the computed and measured shoreline and bathymetry evolution data for Test 11. The presence of the breakwater leads to the formation of two opposing eddies in the area behind it, as currents move towards the sheltered area along the foreshore from both sides of the structure. A secondary cause of the observed circulation pattern is the mean sea level gradient between the illuminated and sheltered areas due to diffraction effects, while the representation of swash zone hydrodynamics by the model should be highlighted (see also Section 2.2).

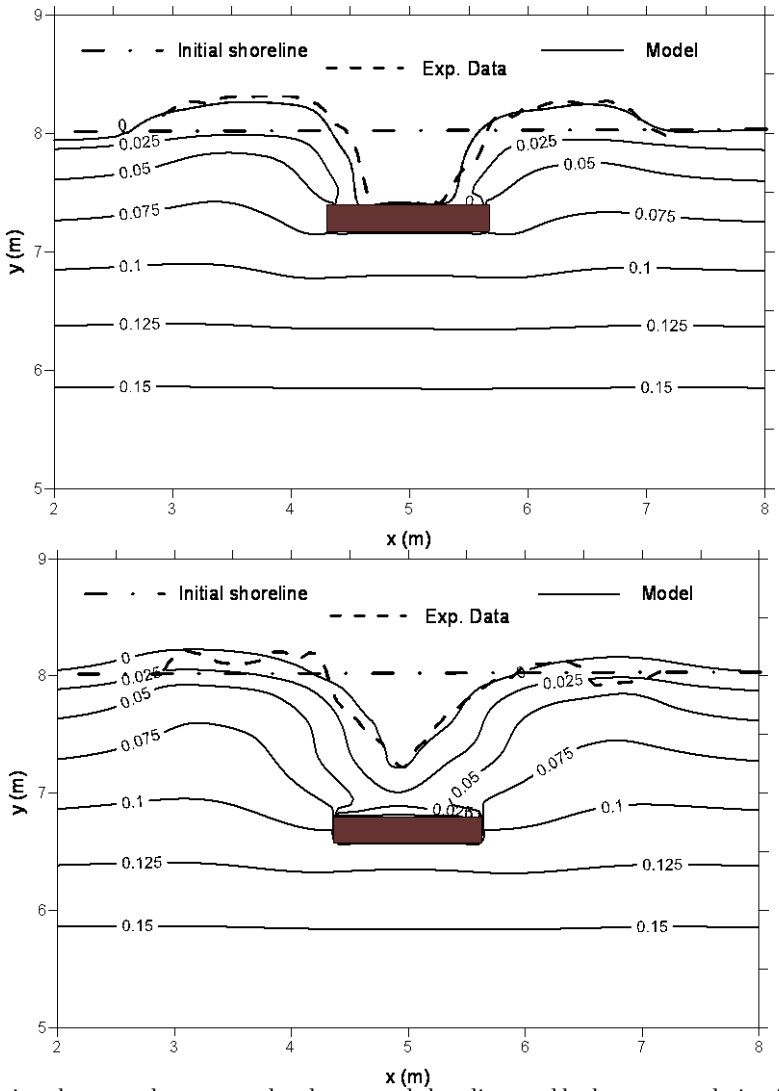

Figure 2: Comparison between the computed and measured shorelines and bathymetry evolution for Test 3 (top) and Test 10 (bottom) of Ming and Chiew (2000).

Regarding morphology evolution, model results are in good agreement with the measure data of Ming and Chiew (2000), capturing the formation of the tombolo in Test 11 (Figure 1, bottom), as well as the formation of the tombolo and salient in Tests 3 (Figure 2, top) and 10 (Figure 2, bottom), respectively.

The present model was also tested against data from the small-scale experiments of Baidei et al. (1994), in which the impact of groins on nearshore morphology was studied under the attack of obliquely incident random waves. The physical model regarded an initially plane sloping beach (1:10 slope), composed of 0.12 mm sand grains. The beach – without the presence of the groins – was exposed to wave action for a duration of 4 h until the formation of a nearly stable bathymetry. The installation of the groins followed, and the tests continued for another 12 h. In this work, the case of a single groin was modelled, exposed to waves of H_{s0}=0.06 m deep water significant wave height, T_p=1.15 s peak period and θ_0=11.6^o deep water incident wave angle. Figure 3 shows the breaking wave-induced current velocity field and the comparison between the computed and measured shoreline and bathymetry evolution for the aforementioned test. The sediment accretion updrift of the groin-type structure results in an advance of the shore, while the lack of sediments at the lee of the groin leads to the shore retreat; bathymetric contours are well-reproduced too, with model results and measurement lines practically overlapping.

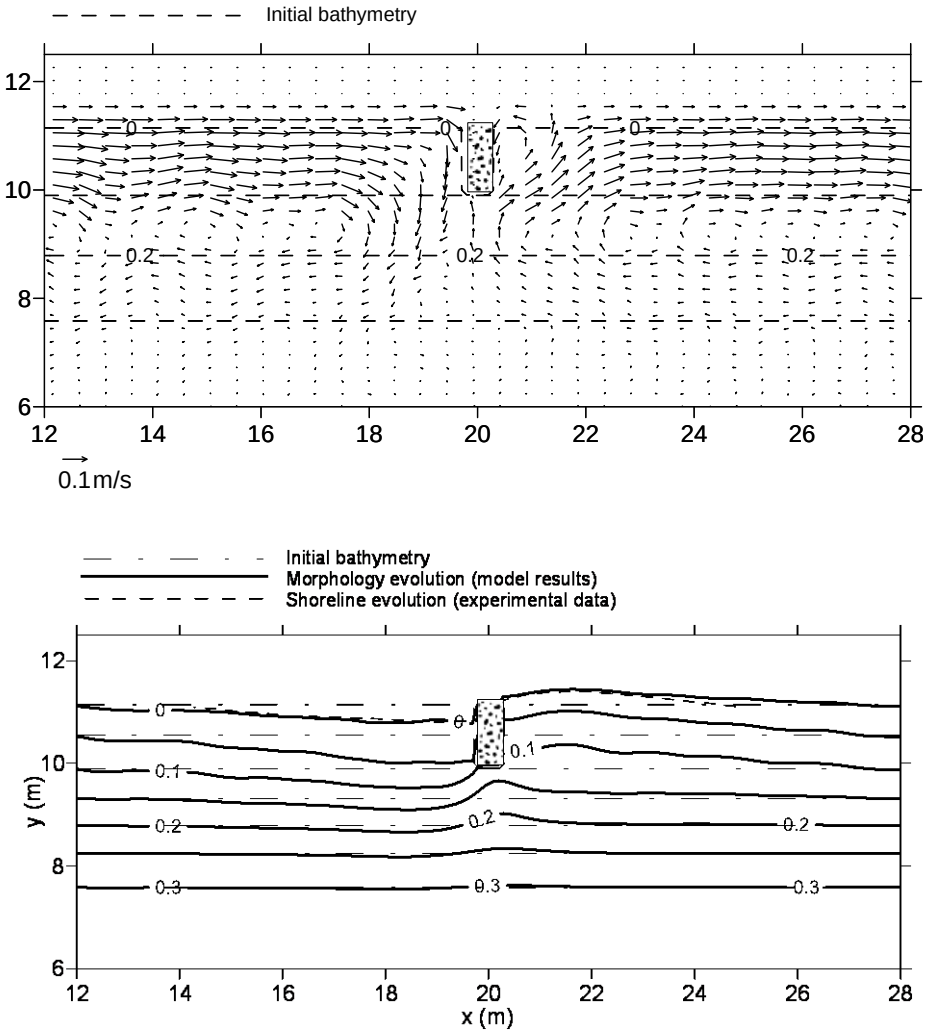

Figure 3: Breaking wave-induced current velocity field and comparison between the computed and measured shoreline and bathymetry evolution due to the presence of a groin (data from Baidei et al., 1994).

3.2. *Comparison with field measurements*

Model verification against field measurements, was achieved by simulating the beach evolution at Sangjun beach (Thailand) where 2D morphological data are available by Chonwattana and Weesakul (2005). The study area, Sangjun beach, is a touristic area located in Thailand. Local authorities constructed fishtail groins to trap the sediment, monitoring the beach morphology before and after the construction, in December 2000 and June 2001, respectively.

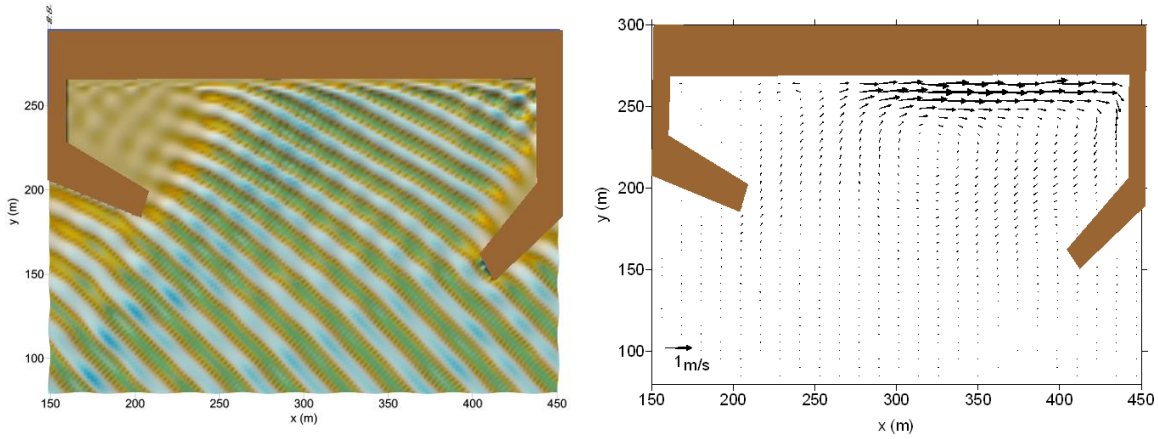

Figure 4: Snapshot of the computed free surface elevation for the first representative obliquely incident wave (H_e=0.69 m, T=3.93 s, θ_0=-45.68°) and resulting wave-induced current velocity field in Sangjun Beach.

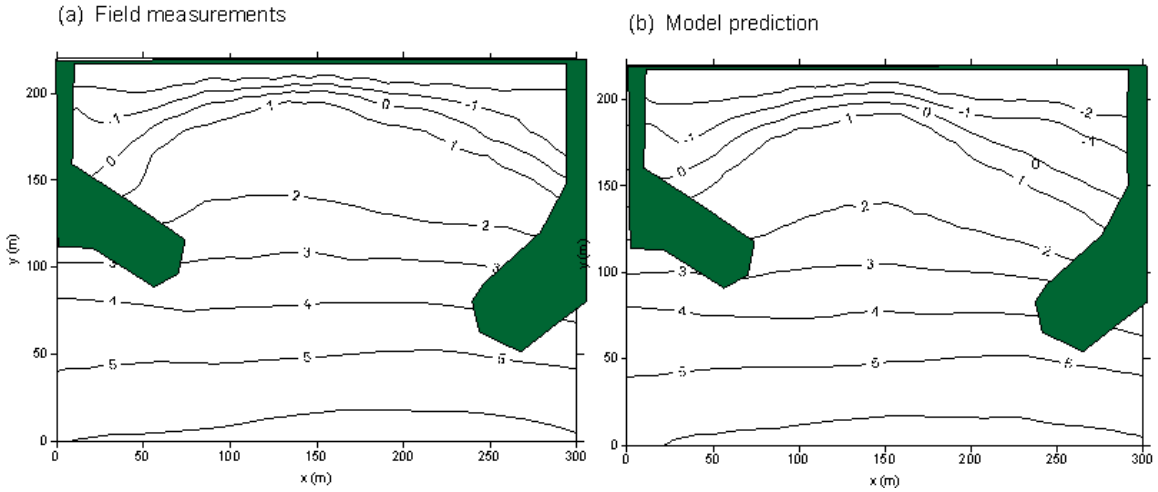

Figure 5: Measured and calculated bed elevation (m from MSL) after the construction of the fishtail groins in Sangjun Beach between (data from Chonwattana et al., 2005).

The integrated model was run for 3 representative waves corresponding to 3 incident directions, as determined by Chonwattana and Weesakul (2005). The workflow for the coupled module runs can be summed-up in the following. Starting with the initial bathymetry, WAVE_L, WICIR and SEDTR modules were run in sequence for the characteristics of the first representative wave and taking into account its annual frequency of occurrence for the simulation of morphology evolution. The updated bed morphology was then used to run the integrated model for the second representative wave (in the same way) and the morphology at the end of this second run for the third representative wave. The aforementioned simulation steps were repeated until the total duration of the wave action was reached.

Figure 4 shows a snapshot of the computed free surface elevation for the first representative obliquely

incident wave (H_e=0.69 m, T=3.93 s, θ_0=-45.68°), as well as the resulting wave-induced current velocity field. Figure 5 shows the comparison between the measured and calculated bed elevation (in m from MSL) after the construction of the groins. The agreement between measured and computed data is quite close, with the integrated model capturing the transformation of the initially straight shoreline and bathymetric contours into a bay-shaped beach.

3.3. *Application to Paralia Katerinis beach (Greece) – Coastal protection with submerged breakwaters*

Following its validation for laboratory and field measurements, the presented integrated model was applied to a real case study of a coastal engineering project regarding the protection of a beach by using detached breakwaters. The study area is located in the Region of Central Macedonia, Greece, at a sandy beach northern of Katerini fishing port (Figure 6). The area has been facing coastal erosion problems for well over 30 years, which started after the construction of the harbour seen in the left part of Figure 6 (1980 to 1984). As a result, and due to the prevailing SE winds, the coastal zone south from the fishing port showed strong accretion while the coast north from the port was eroded, with a shoreline retreat at the order of 20 m; the erosive phenomena stretched over a zone of 800 m north from the port. In order to reverse erosion, a groin field consisting of 13 rubble mount groins, was constructed (1990 to 1997). The project not only failed to further protect the beach – since additional erosion occurred in between the constructed groins – but it also transferred coastal retreat northwards. Furthermore, the semi-closed basins that formed between the constructed groins, being in the non-tidal Mediterranean Sea, caused significant environmental problems regarding water quality due to the limited renewal rates. In 2010 a new coastal protection project was designed and constructed; the groin field was replaced by a set of three 200 m long submerged breakwaters placed at a distance of approximately 200 m from the coast, the gaps between the structures being of approximately 110 m. The breakwaters were designed to have transmission coefficients in order of 0.4 (K_t≈0.4). In addition, a beach nourishment project was also designed and applied to restore the beach to its previous condition. Bathymetry measurement data for the area are available for the period right after the completion of coastal works (beach nourishment and construction of the submerged breakwaters), as well as for 3 years later (Christopoulos, 2014). The integrated model was applied to simulate coastal morphodynamics after the realization of the coastal protection project. Since wave data were not available at the area, a hindcast data were used. The main incident wind directions are: NE, E and SE. The model was run by applying as forcing 3 representative waves (i.e. 3 equivalent wave heights on an annual basis).

Figure 7 shows the breaking wave-induced current field for the prevailing SE waves. Submerged breakwaters allow some wave transmission and overtopping which cause an additional supply of water in the lee of the structure, which affect the current field. This net transport of water into the lee zone causes a water level rise and is balanced mainly by outgoing currents at the heads of the structures. Consequently the main flow pattern is characterized by an onshore flow over the submerged breakwater, an offshore flow at the gaps (eroding rip currents) and nearshore eddies similar to those formed in the case of emerged breakwaters. The first two flow patterns do not exist in the latter case, while the third flow pattern is not extended up to the structure.

Figure 6: Location and satellite image of the study area at Paralia Katerinis (Google Earth, 2017; privately processed).

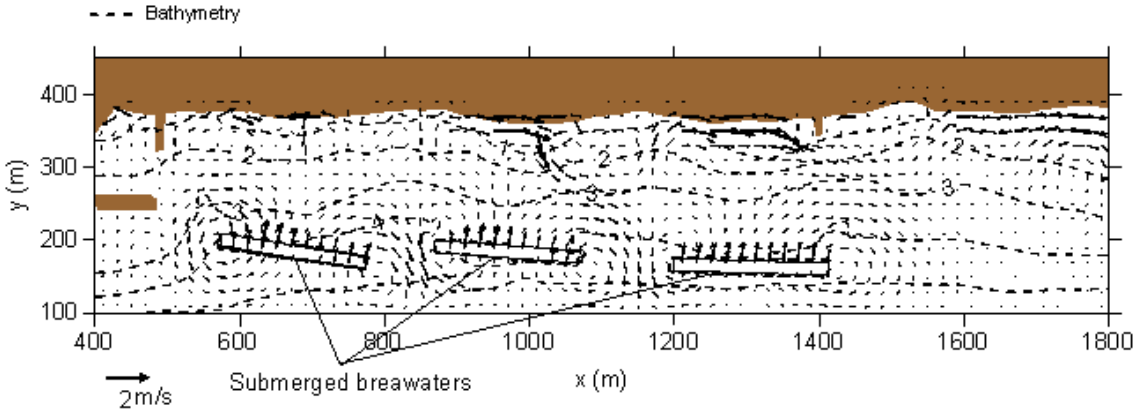

Figure 7: Breaking wave-induced current field for the prevailing SE waves.

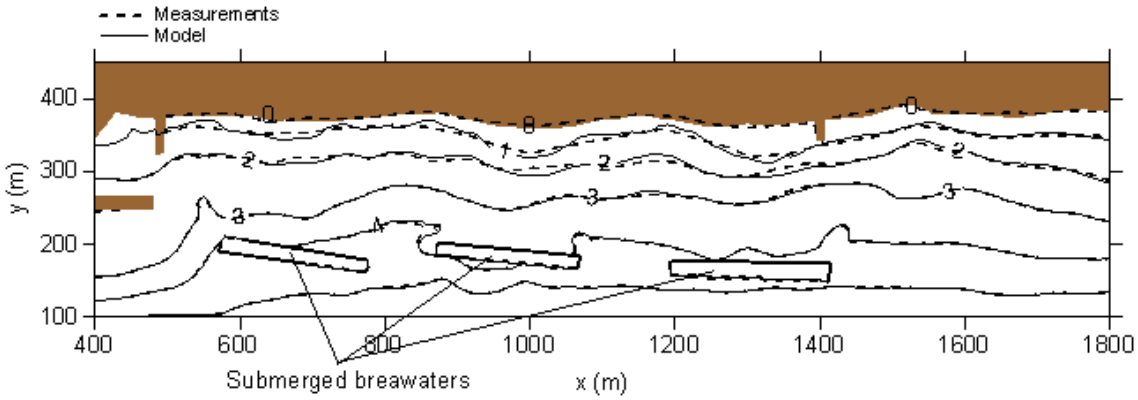

Figure 8: Calculated and measured bed morphology evolution of Paralia Katerinis coast

The workflow for the coupled module runs is identical to the one described for the model validation runs in Section 3.2, resulting in the final morphology evolution at the study area shown in Figure 8.

4. Conclusions

Integrated modelling has become an essential need for modern coastal engineering design. The model presented in this work consists of three modules that simulate linear wave propagation, wave-induced circulation and morphology evolution, and it is tested against experimental data to study the effect of representative coastal protection structures, such as detached breakwaters and groins. Given the good agreement between model results and laboratory measurements, the model was also successfully applied to a real case study of two coastal engineering projects in Thailand (fishtail groins) and North Greece (submerged breakwaters). The model is deemed to constitute a suitable tool for the design and evaluation of the morphological influence of harbour and coastal protection works, being able to deliver results in a fast and seamless way at all times for a wide range of design layouts.

References

Badiei, P., Kamphuis, J.W. and Hamilton, D.G, 1995. Physical experiments on the effects of groins on shore morphology, *Coastal Engineering 1994*, 128: 1782-1796.

Baba, Y. and Camenen, B., 2007. Importance of the Swash Longshore Sediment Transport in Morphodynamic Models,

Coastal Sediments 07, http://dx.doi.org/10.1061/40926(239)152.

Battjes, J.A., 1975. Modelling of turbulence in the surf zone, *Symposium on Modelling Techniques, ASCE*, 1050-1061.

Battjes J. A. and Janssen, J. P. F. M. (1978). Energy Loss and set-up due to breaking of random waves, *Coastal Engineering 1978*, 569-587.

Camenen, B., Larson, M., 2006. Phase-lag effects in sheet flow transport. *Coastal Engineering*, 53: 531-542.

Camenen, B. and Larson, M., 2007. *A unified sediment transport formulation for coastal inlet application*. Technical Report ERDC/CH: CR-07-1, US Army Corps of Engineers, Engineering Research and Development Center, Vicksburg, MS, USA.

Camenen, B., Larson, M., 2008. A general formula for noncohesive suspended sediment transport, *Journal of Coastal Research*, 24(3): 615-627.

Chonwattana, S., Weesakul, S. and Vongvisessomjai, S., 2005. 3d modeling of morphological changes using representative waves. *Coastal Engineering Journal*, 47(4): 205-229.

Christopoulos, S. (2004). *Coastal protection works of Paralia Katerinis*. Technical Report, Municipality of Katerini, Greece (in Greek).

Copeland, G.J.M., 1985a. A practical alternative to the "mild-slope" wave equation. *Coastal Engineering*, 9(2): 125-149.

Copeland, G.J.M., 1985b. Practical radiation stress calculations connected with equations of wave propagation. *Coastal Engineering*, 9(3): 195-219.

De Vriend H. J. and Stive M. J. F., 1987. Quasi-3D modelling of nearshore currents. *Coastal Engineering*, 11: 565-601.

Google Earth (2016). Image ©2016 TerraMetrics, Data SIO, NOAA, U.S. Navy, NGA, GEBCO.

Isobe, M. and Horikawa, K., 1982. Study on water particle velocities of shoaling and breaking waves. *Coastal Engineering in Japan*, 25: 109-123

Karambas, Th.V. and Bowers E.C., 1996. Representation of partial wave reflection and transmission for rubble mound coastal structures. *WIT Transactions on Ecology and the Environment*, 12: 415-423.

Koutandos E.V., Karambas, Th.V. and Koutitas, C.G., 2004. Floating breakwater response to waves action using a Boussinesq model coupled with a 2DV elliptic solver. *Journal of Waterway, Port, Coastal and Ocean Engineering*, 130(5): 243-255.

Kriezi E. and Karambas, Th.V., 2010. Modelling wave deformation due to submerged breakwaters. *Maritime Engineering*, 163(1): 19-29.

Kobayashi N. and Tega Y., 2002. Sand suspension and transport on equilibrium beach. *Journal of Waterway, Port, Coastal, and Ocean Engineering*, 128(6): 238-248.

Kobayashi, N., Agarwal, A. and Johnson, B., 2007. Longshore Current and Sediment Transport on Beaches. *Journal of Waterway, Port, Coastal, and Ocean Engineering*, 133(4), 296-304.

Militello A., Reed, C.W., Zundel, A.K. and Kraus, N.C., 2004. *Two-Dimensional Depth-Averaged circulation model M2D: version 2.0, Report 1*, US Army Corps of Engineers, ERDC/CHL TR-04-2.

Larsen, J. and Dancy, H., 1983. Open Boundaries in Short Wave Simulations - A New Approach. *Coastal Engineering*, 7: 285-297.

Lee C. and Suh, K.D., 1998. Internal generation of waves for time-dependent mild-slope equations. *Coastal Engineering*, 34: 35-57.

Larson, M. and Wamsley, T.V., 2007. A formula for longshore sediment transport in the swash. *Coastal Sediments '07*, 1924-1937.

Ming, D. and Chiew, Y., 2000. Shoreline changes behind detached breakwater. *Journal of Waterway, Port, Coastal, and Ocean Engineering*, 126(2): 63-70.

Nam, P.T., Larson, M., Hanson, H. and Hoan, L.X., 2009. A numerical model of nearshore waves, currents, and sediment transport. *Coastal Engineering*, 56: 1084-1096.

Watanabe A. and Maruyama K., 1986. Numerical modelling of nearshore wave field under combined refraction, diffraction and breaking. *Coastal Engineering in Japan*, 29: 19-39.